Recent Results from Internal and Very-Near-Field Plasma Diagnostics of a High Specific Impulse Hall Thruster

Richard R. Hofer*
QSS Group, Inc.
Cleveland, OH 44135 USA
richard.hofer@grc.nasa.gov

Alec D. Gallimore†
Plasmadynamics and Electric Propulsion Laboratory
University of Michigan
Ann Arbor, MI 48109 USA

ABSTRACT

Floating potential and ion current density measurements were taken on the laboratory model NASA-173Mv2 in order to improve understanding of the physical processes affecting Hall thruster performance at high specific impulse. Floating potential was measured on discharge chamber centerline over axial positions spanning 10 mm from the anode to 100 mm downstream of the exit plane. Ion current density was mapped radially up to 300 mm from thruster centerline over axial positions in the very-near-field (10-250 mm from the exit plane). All data were collected using a planar probe in conjunction with a high-speed translation stage to minimize probe-induced thruster perturbations. Measurements of floating potential at a xenon flow rate of 10 mg/s have shown that the acceleration layer moved upstream 3±1 mm when the voltage increased from 300 V to 600 V. The length of the acceleration layer was 14±2 mm and was approximately constant with voltage and magnetic field. Ion current density measurements indicated the annular ion beam crossed the thruster centerline 163 mm downstream of the exit plane. Radial integration of the ion current density at the cathode plane provided an estimate of the ion current fraction. At 500 V and 5 mg/s, the ion current fraction was calculated as 0.77.

I. INTRODUCTION

Expanding the operating envelope of Hall Effect Thruster (HET) technology has been the subject of several investigations conducted at the NASA Glenn Research Center (GRC).[1] As part of this program, research on the physical limits of HETs—in terms of power and specific impulse (Isp)—is being conducted. Separate studies at GRC have demonstrated power levels of 72 kW and Isp of 4100 s with xenon HETs.[2-3] This paper discusses continuing efforts at GRC to develop efficient, high-Isp thrusters.

Most recently, these efforts have resulted in the development of two different laboratory model HETs, the NASA-173Mv1 and the NASA-173Mv2, both of which were built to investigate high-Isp phenomenon. The hypothesis when building the thrusters was that the magnetic field topography required for efficient, high-voltage operation would differ from that employed at 300 V. Therefore, the thrusters use magnetic circuits allowing for significant variations of the field topography. Performance characterizations of both thrusters have confirmed the hypothesis.[4-5] While other thrusters have exhibited maximum efficiencies in the range of 500–800 V, an efficiency that increases monotonically with voltage has been demonstrated in the 173Mv2.[3,5,6,7] Experiments have shown that efficient operation in the 3000 s range of Isp is possible if a minimum current density is maintained and the magnetic field topography is properly shaped.[5]

While the 173Mv2 can be operated at efficient, high-Isp conditions, an understanding of the physical mechanisms driving performance is needed to address lifetime requirements. It has been shown that current density and field topography are critical to improving efficiency, therefore it is necessary to identify the processes that are affected when these variables are changed.[5] Such an understanding is required to design higher-fidelity thrusters with lifetimes sufficient for near-Earth and interplanetary missions. To that end, a series of probe diagnostics were deployed to help improve the understanding of competing mechanisms affecting HET performance at high specific impulse.

In this paper, recent measurements of floating potential and ion current density using a planar probe are reported. Floating potential was measured over axial sweeps on discharge chamber centerline. The ion current density was mapped axially in the very-near-field (VNF) 10–250 mm downstream of the thruster exit plane and at radial positions extending 300 mm from thruster centerline. In the following, an overview of the experimental apparatus is first discussed, followed by analyses of results from the measurements.

---

* Research Scientist
† Associate Professor, Associate Fellow AIAA

II. EXPERIMENTAL APPARATUS

A. NASA-173Mv2 Hall effect thruster

The laboratory model NASA-173Mv2 is a 5 kW-class Hall thruster that has a discharge chamber outer diameter of 173 mm (Figure 1; see Ref. 5 for a detailed description). A fixed structure of magnetic poles pieces, an inner coil (IC) and an outer coil (OC) are used to form the primary magnetic circuit. Fine control of the magnetic field is provided with an internal trim coil (ITC) and an external trim coil (ETC). The ITC primarily affects the radial magnetic field in the discharge chamber, while the ETC affects the magnetic field downstream of the exit plane and near the cathode. Throughout this paper, operation without the ITC or ETC is referred to as "No TC's," meaning that only the IC and OC were used.

The plasma discharge was powered by a matching pair of commercially available power supplies wired in series that provided a 1200 V, 16 A output. The discharge filter consisted of a 95 μF capacitor in parallel with the supply outputs and a 1.3 Ω resistor in series with the positive terminal of the supply output. Other laboratory supplies were used to power the magnet coils, cathode heater and cathode keeper.

Xenon (99.999% pure) was supplied through stainless steel feed lines with 20 sccm and 200 sccm mass flow controllers. The controllers were calibrated before testing using a constant-volume method.

A GRC laboratory model hollow cathode rated for 20 A, which was located above the thruster, was used in the experiments (Figure 1). Probe measurements were performed in the horizontal plane on the thruster centerline, which was perpendicular to the vertical plane of the cathode.

The thruster was operated for 2–4 hours after initial exposure to vacuum conditions to allow for outgassing of the chamber walls. Upon subsequent thruster shutdowns and restarts, the 173Mv2 was operated for at least 30 minutes before data was acquired. This allowed enough time for the discharge current to reach a steady-state value.

B. Vacuum facility

All experiments were conducted at the University of Michigan's Plasmadynamics and Electric Propulsion Laboratory (PEPL) in the Large Vacuum Test Facility (LVTF). A schematic of the facility is shown in Figure 2. The LVTF is a stainless steel vacuum chamber that measures 6 m in diameter and 9 m in length. The thruster was mounted at the "probe table" location, as indicated in the schematic, and fired away from the cryopumps.

The LVTF was equipped with seven cryopumps that produced a pumping speed of 240,000 l/s on xenon and an ultimate base pressure of 2.5×10^{-7} Torr. Chamber pressure was monitored using two hot-cathode ionization gauges mounted on the chamber walls. Pressure measurements for each gauge were corrected for xenon using the base pressure on air and a correction factor of 2.87 for xenon. For the results reported here, the facility was operated with either four or seven cryopumps. The pressure, with a xenon flow rate of 5.5 mg/s and seven pumps operating, was 4.5×10^{-6} Torr; with four pumps and a flow rate of 11 mg/s, the pressure was 1.3×10^{-5} Torr. (The rationale for operating either four or seven pumps is discussed at the beginning of section III.)

C. Positioning system

To position the planar probe with respect to the thruster, three translation stages were used. The thruster was mounted on a two-axis positioning system that primarily provided radial positioning. (These stages are indicated as the "probe table" in Figure 2.) Axial sweeps of the probe were done with the probe attached to the PEPL High-speed Axial Reciprocating Probe (HARP) positioning system (Figure 2; for a full description, see Ref. 8-10). The system was used to rapidly move the probe in and out of the thruster discharge chamber and plume to minimize probe-induced thruster perturbations. The total sweep time (in and out) averaged 300 ms over an axial length of 254 mm. Thruster perturbations always began inside the cathode plane (see section III.A.1). When positioned on the discharge chamber centerline, the sweep time in one direction from the cathode plane to 10 mm from the anode (58 mm total) ranged from 38–41 ms. Thus, the probe never spent more than 82 ms in this region of the thruster.

A single coordinate system was defined for all measurements. Axial positions were referenced from the exit plane, with the anode at z = –38 mm and the cathode plane at z = +30 mm. Radial positions were referenced from the thruster centerline, with the discharge chamber centerline at r = 73.7 mm and the outer radius of the thruster body at r = 135 mm.

D. Planar probe

A planar probe, consisting of a 1.54 mm diameter tungsten electrode flush with one end of a

99.8%-pure alumina jacket, was used to measure both floating potential and ion current density. The outer diameter of the alumina jacket was 3.24 mm. Over the measurement domain, the Debye length ranged from 0.04–0.08 mm, which was much less than the electrode diameter.[10] Thus, the effective collection area was taken as the geometric area. Similar designs have been used in ion current density studies of the D-55 and SPT-100.[11-12]

1. Floating potential

The relative simplicity of measuring the floating potential is preferred to using failure-prone emissive probes to measure the plasma potential when considering changes to a thruster configuration (e.g. voltage, current, geometry, magnetic field). Esipchuk, Bishaev, Raitses and Kim have used measurements of the floating potential to gain insight on the acceleration process.[13-16] It has been shown that transient fluctuations of the floating potential were followed by the plasma potential and that the stationary values of the two quantities follow very similar trends.[13,16]

In an unmagnetized, quiescent, Maxwellian plasma, the floating potential (V_f) is related to the plasma potential (V_p) by:

$$V_f = V_p - \frac{kT_e}{e}\frac{1}{2}\left[1 - \ln\left(\frac{2\pi m_e}{M_i}\right)\right] \qquad \textbf{(1)}$$

(where T_e is the electron temperature, k is the Boltzmann constant, e is the elementary charge, m_e is the electron mass and M_i is the ion mass).[17] This is an important relationship because it is the plasma potential, or more specifically, the electric field derived from it, that accelerates the ions in a HET. The presence of magnetic fields, streaming ions and non-Maxwellian velocity distributions inside a HET complicates the relationship between the floating and plasma potential, such that Eq. 1 is not strictly valid. However, the error is on the order of the electron temperature (10–40 eV in a HET) so the floating potential profile is still a useful, albeit inexact, representation of the plasma potential.[10]

The accuracy of a floating potential measurement in the presence of magnetic fields is determined by two important factors: the ratio of the electron or ion Larmor radius to the probe radius and the orientation of the probe with respect to the magnetic field lines.[17] To achieve acceptable results, the probe radius should be less than the electron Larmor radius and oriented such that the magnetic field lines are nearly perpendicular to the collection electrode. This orientation allows particles to flow freely to the probe.

As a basic operating principle of HETs, the magnetic field and channel dimensions are chosen so that only the electrons are magnetized.[18] The relationship between the ion and electron Larmor radii (R_{Li} and R_{Le}) is therefore:

$$R_{Li} >> L >> R_{Le} \qquad \textbf{(2)}$$

(where L is a characteristic channel dimension, usually the channel width). Since the electrons are magnetized while the ions are essentially unperturbed by the magnetic field, the probe radius should be smaller than R_{Le}. For these experiments, R_{Le} was estimated to range from 1–5 mm, while the probe radius was 0.77 mm. While the accuracy of the measurement would improve with a smaller probe, the error was deemed acceptable for the present application.

The probe was oriented with the collection electrode parallel to the radial direction. While the magnetic field lines on the centerline were essentially radial, there was always an axial magnetic field that canted the field lines. This fact, combined with inaccuracies of aligning the probe, imply that there was always a flux of electrons that were allowed to freely stream to the probe. It was also thought that anomalous diffusion of the electrons across magnetic field lines enhanced the flux of electrons to the probe, even in regions of negligible axial magnetic field.

With these considerations, the measurement uncertainty of the floating potential was estimated as ±10%. This estimate included the effects of probe-induced thruster perturbations (see section III.A.1). To make the measurements, the electrode was isolated from ground and allowed to float. A 100X, 10 MΩ voltage probe connected to a 500 MHz oscilloscope was used to measure the floating potential with respect to ground. Combined with a simultaneous measurement of the cathode potential with respect to ground, the floating potential of the probe with respect to the cathode was then computed.

2. Ion current density

To measure ion current density, the planar probe was biased –15 V below ground to repel electrons. The bias voltage was determined based on the results of a probe bias study (see section III.B.1). The current collected by the probe was determined by measuring the voltage drop across a 508 Ω precision resistor using an isolation amplifier, the output of which was connected to a 300 MHz oscilloscope. A guard ring was omitted from the probe for the sake of simplicity, which

increased the collected current due to edge effects and charge-exchange (CEX) ion collection. (An attempt to correct for CEX is discussed in section III.B.3.) To account for secondary electron emission, data from Hagstrum was used for singly-charged xenon bombardment on tungsten, which showed a nearly constant correction factor of 0.018 for ion energies up to 1000 eV.[19] Finally, the probe was always oriented such that the electrode was parallel to the thruster exit plane. At large radial positions from centerline, there were some attendant cosine losses. Since beam divergence was still relatively minor even at the largest radial and axial coordinates (r,z = 300, 250 mm), these losses were ignored.

III. RESULTS AND DISCUSSION

Floating potential data were collected at 300 V and 600 V, at a constant flow rate of 10 mg/s and with different magnetic field configurations. These data were taken when only four cryopumps were used (during initial troubleshooting). The ion current density data was taken at 500 V, 5 mg/s but with seven cryopumps running. Probe failure and time constraints prohibited further data collection of either ion current density or floating potential. Thruster telemetry during data collection for both measurements is shown in Table 1. For reference, the thrust, specific impulse and efficiency from a performance characterization conducted at NASA GRC, are also included.[5]

A. Floating potential

Results from floating potential measurements on discharge chamber centerline (r = 73.7 mm) are presented in Figures 3–7. Only data from sweeps into the thruster are shown. The thruster was operated at a constant mass flow rate of 10 mg/s and the discharge voltage was either 300 V or 600 V. Changes to the magnetic field were investigated by using different combinations of the trim coils. The coil currents were taken from a performance characterization that showed these settings maximized efficiency.[5] Axial positions were referenced from the exit plane, with the anode at z = –38 mm and the cathode plane at z = +30 mm.

1. Probe-induced thruster perturbations

Inserting the probe into the discharge chamber was found to affect thruster operation by increasing the discharge current and the cathode potential (Figures 3 and 4; the floating potential is included for reference only and will be discussed in subsequent sections). The thruster was operated at 300 V or 600 V at a constant flow rate of 10 mg/s and both the ITC and ETC were energized. At both voltages, the discharge current and cathode potential began to increase when the probe reached z = +15 mm. Upon removal of the probe (not shown in Figures 2 and 3) the current and cathode potential returned to their initial steady-state values. At 300 V, the current increased by 45% and at 600 V by 38%.

The percentage change in the discharge current was much greater than expected, based on prior experiments on the 5 kW P5 Hall thruster that also used the HARP.[10] In Ref. 10, discharge current perturbations were less than 10% when operating at 10 A, 300 V. The experiments with the P5 and 173Mv2 were similar in three important aspects: first, the thrusters shared discharge chamber geometry. Second, in Ref. 10 a double probe that was 3.2 mm long by 1.6 mm wide was used, which was just slightly smaller than the 3.4 mm diameter floating probe used on the 173Mv2. Third, the probes in Ref. 10 moved more slowly than the floating probe used here. The faster the probe moved, the less susceptible the probe body was to ablation, which is known to affect thruster operation.[8]

The one major difference between the experiments was in the applied magnetic fields. It was hypothesized that the magnetic field in the 173Mv2 improved plasma confinement as compared to the P5. This would have raised the plasma density in the discharge chamber and made the 173Mv2 more susceptible to disturbances caused by probes. The hypothesis that the plasma density was higher in the 173Mv2 than in the P5 was supported by the improved efficiency and plume characteristics of the 173Mv2 compared to the P5.[5,20,21] Since the 173Mv2 probe was slightly larger than the probe used on the P5, a smaller probe should reduce the magnitude of disturbances. Future experiments with smaller probes will test this hypothesis.

The disturbances to thruster operation increased the uncertainty of the floating potential measurements, which was estimated to be ±10%. This included the uncertainty associated with the probe design (see section II.D.1).

2. Effects of the magnetic field on the floating potential

Figures 5 and 6 show how changes to the magnetic field affected the floating potential at 300 V and 600 V, respectively. At both voltages, changing the magnetic field by using the ETC increased the floating potential by 10–15 V at distances greater than z = +10 mm. In Ref. 5, the

ETC generally increased the cathode potential[#] (i.e., decreased the magnitude with respect to ground) and increased the plume divergence. This indicated that changes to the external magnetic field were primarily affecting the electron coupling with the discharge, rather than improving ion focusing. The floating potential data supported this conclusion by demonstrating that the VNF floating potential was increased with the ETC, which would improve the coupling of the electrons with the discharge chamber plasma.

The effect of the ITC on the potential distribution was less apparent than the ETC, mostly likely because of the way the ITC changed the magnetic field. The ITC primarily altered the axial gradient of the radial magnetic field, which changed the radius of curvature of the field lines. Thus, the effects of the ITC would be more noticeable by comparing the potential distribution radially across the discharge chamber. Also, the ITC reduced the fall potential at the anode by zeroing the magnetic field.[4] Neither of these effects can be resolved by the data in Figures 5 and 6.

As shown in Figure 6, there was a local maximum in the potential distributions that occurred at z = +6 mm. The trim coils decreased the prominence of this feature. Figure 4 also shows disturbances to the discharge current at this same location. Similar results were reported on the P5 with both emissive and floating probes, but a complete explanation for the effect was not determined.[9] In the absence of other data, these features are most likely the result of the probe perturbing the plasma. Non-perturbing laser diagnostics are ideally suited to diagnose whether or not this is an artifact of the probe disturbing thruster operation.

3. Effects of the discharge voltage on the floating potential

Figure 7 compares operation at 300 V and 600 V when both the ITC and ETC were energized. (The other data were excluded for clarity.) The negative first derivative of the floating potential ($-dV_f/dz$) was computed by numerical differentiation, under the assumption that this quantity was proportional to the axial electric field (E_z). As shown in Figure 7, the magnitude of $-dV_f/dz$ at 600 V was roughly twice the value at 300 V. To first order the axial electric field scales as $E_z \propto V_D/L_a$, where V_D is the discharge voltage and L_a is the thickness of the accelerating layer. Thus, these results suggested that the accelerating layer thickness was weakly dependent on voltage. This was expected because, at both operating conditions, the position of the anode and cathode were unchanged and the axial gradient of the magnetic field was approximately the same.

When analyzing all the data from Figures 5 and 6, the results indicated that the acceleration layer thickness was 14±2 mm, which closely agreed with experimental and theoretical values.[18,22] There was no strong dependence on voltage or magnetic field, but this result may have been obscured by measurement uncertainty. The thickness was defined as the distance separating the points on either side of the maximum value of $-dV_f/dz$ that equaled 10% of the peak, excluding the regions at 600 V where the electric field was negative. Alternatively, if the acceleration layer thickness was defined by the distance separating the points where the electric field initially increased above zero and where it returned back to zero (again excluding the negative regions at 600 V), then the layer thickness was about 40 mm. Thus, while the bulk of the acceleration occurs over a short distance of 14 mm, the ions reached their maximum velocity over a length of 40 mm. Also, it was observed that the potential reached a minimum at the cathode plane (z = +30 mm). In the P5 HET, the cathode plane was at z = +50 mm and this was where the potential reached a minimum.[10] This implies that the acceleration layer thickness can be partially dictated by cathode placement, which has implications on controlling divergence, decreasing erosion and improving efficiency.

As shown in Figure 7, the acceleration layer shifted closer to the anode at 600 V, by 3±1 mm when all data was considered. This result was supported by visual observations of the plasma shifting closer to the anode as the voltage increased.[5] A shift in the acceleration layer position affects thruster lifetime because shifts towards the anode increase the likelihood of radial electric fields accelerating ions into the wall. Since efficiency increased between 300 V and 600 V, it may be that such effects are offset by improved focusing efficiency at higher voltages so that erosion rates are not significantly changed.[5] This could partially explain why the 500 V T-220 had nearly the same volumetric erosion rates as the 300 V SPT-100.[23]

B. Ion current density

Previous investigations of high-voltage HETs have shown a general trend of increased discharge current with voltage at constant mass

[#] In these experiments, the cathode potential was more negative when the ETC was used. This was attributed to differences in the vacuum facilities at PEPL and GRC.

flow rates.[3-7] This may have been due to increased electron current and/or multiply-charged ion species. It is important to identify the mechanisms that determine the voltage dependence of the discharge current in order to improve thruster performance and lifetime. Quantifying multiply-charged species, which is best done with an ExB probe, was not considered in these studies.[12] An ion current density measurement is, at least in principle, one way to determine the electron current. By making a measurement of the ion current density and then integrating the profiles, it is possible to calculate the total ion current, which, in turn, determines the electron current since the discharge current is known.

In this section, results are reported from an ion current density mapping at 500 V, 5 mg/s. The goal of these initial experiments was to determine appropriate methods for computing the total ion current. Future measurements will expand the operating conditions to 300–1000 V and 5–10 mg/s so that the voltage and flow rate dependence of the ion current, and therefore the electron current, can be determined.

1. Probe bias study

Before taking data, the effects of the bias voltage were quantified by positioning the probe at several axial positions (z = 10–250 mm) and either on the thruster centerline (r = 0 mm) or on the discharge chamber centerline (r = 73.7 mm). The thruster was operated at 300 V, 5 mg/s for these measurements. Time constraints did not allow for conducting the study at 500 V, 5 mg/s (the condition later reported). At each sampling location, the probe bias was varied from 0 V to –100 V below ground, with the goal of determining a bias voltage that would yield ion saturation without significant sheath growth. Previous studies at PEPL have shown that a bias voltage of –15 V to –20 V was a good choice for HET plumes when sampling at one meter from the exit plane.[24]

Figure 8 shows partial results from the probe bias study that plots ion current density versus probe bias at axial positions of z = +30 or +100 mm at the two radial positions. In general, ion saturation was obtained when the probe was exposed to the main ion beam, as shown at z = +30 mm on the discharge chamber centerline and z = +100 mm on the thruster centerline. When moved to regions where the directed flux of ions was absent, the characteristic generally increased at nearly constant slope, as shown by the other two plots in Figure 8.

The conclusion drawn from the data was that the probe was collecting significant portions of CEX ions in these regions. When not in the exhaust beam, the ion density was depressed, which caused the sheath thickness around the electrode to grow. This, in turn, increased the effective collection area and CEX ion collection. Overall, it was concluded that –15 V bias potential achieved ion saturation without collecting significant CEX current. This was still true up to z = +10 mm on centerline, where electron temperatures are between 5-10 eV.[11-12] At first, it was thought that the probe must have collected some electrons at –15 V bias voltage when the electron temperature was high. The floating potential profiles in Figures 5 and 6 show why this was not the case. At z = +10 mm, the floating potential was between 30–80 V with respect to the cathode for the 300 V and 600 V data. Thus, the potential difference between the probe and the plasma potential (after correcting for the electron temperature) was between 60–110 V. Thus, for electron temperatures of 5-10 eV, there was still a large repelling potential at z = +10 mm. Consequently, most of the electrons were rejected from the electrode and saturation of the probe characteristic was observed.

2. Mapping the ion current density

A single mapping of the ion current density at 500 V, 5 mg/s without trim coils has been conducted and the data analyzed. Data were sampled from the thruster centerline to a radial position of 300 mm. Axial sweeps with the HARP came no closer than 10 mm to the thruster. At r = 145 mm (10 mm past the thruster body), the probe was extended past the thruster body to z = –4 mm. The radial spacing between axial sweeps was 5 mm from centerline to r = 150 mm, and was increased to 10 mm from r = 150–300 mm. The axial spacing between data points was between 1.4–2.7 mm, depending on the probe velocity.

Figures 9 and 10 are contour plots of the ion current density. Figure 9 covers the entire domain that was sampled, while Figure 10 highlights some of the VNF features. Since the oscilloscope sampled at ~1.7 kHz, it was possible to resolve some of the current oscillations. When the probe was stationary, the collected current had a standard deviation of ±10–20% of the mean. This variability was on the order of the discharge current oscillations, which were measured in a different study.[5] To account for the oscillations and approximate the mean, cubic splines were used to curve-fit each sweep. Perturbations introduced by the probe during the ion current density measurements were similar to the floating potential probe (see Figures 3 and 4). However, since the

probe did not go past z = +10 mm, the disturbances were substantially reduced.

As shown in Figure 9, the VNF structure of the plume was similar to ion current density measurements of the SPT-100 and D-55 and to emission spectroscopy of the SPT-100ML.[11,12,25] The ion beam had a noticeable cant towards the thruster centerline after exiting the discharge chamber. A maximum ion current density of 76 mA/cm^2 at z = 163 mm was reached on thruster centerline. The peak current density coincided with the point where the main exhaust beam appeared to cross the centerline. This was unexpected because angular profiles of the ion current density from the 173Mv2 at z = 985 mm have shown a double peak profile that was attributed to the annular discharge chamber.[5] In Ref. 5, the double peaks were each 3° from centerline, which equates to an arc length of 50 mm.

The average radial velocity required for the beam to reach thruster centerline at z = 163 mm was estimated. The axial ion velocity was calculated as 26 km/s, which assumed a 450 V effective accelerating potential. The ion beam was assumed to have originated from the chamber centerline (r = 73.7 mm). The average radial velocity was then computed as 12 km/s, or 46% of the axial velocity. This was a substantial portion of the axial velocity, but still in agreement with laser-induced fluorescence measurements of the radial ion velocity in the P5.[26] The P5 measurements were made at 300 V, 10 A on the thruster centerline. While the operating condition of the P5 was different from that of the 173Mv2, the results should be comparable because the geometries are similar. In the P5 study, the radial velocity was 7.4–8.5 km/s at z = 100 mm and decreased to 1.8–2.0 km/s by z = 500 mm. The reduction of radial velocity with axial position may explain why the ion current density peaks were observed ±50 mm radially from the centerline in the 173Mv2 at z = 985 mm. To check this, the average radial velocity was estimated from the geometry and an axial velocity of 26 km/s. The results showed that in order for the beam to diverge from the centerline at z = 163 mm to the observed peaks at (r,z) = ±50, 985 mm, the average radial velocity would have been 1.6 km/s. This value was very close to the radial velocity observed in the P5 at z = 500 mm. While the trends in the 173Mv2 ion current density are in close agreement with the P5 velocity measurements, the mechanism responsible for the change in radial velocity with axial position is not known.

The dynamics of the beam in the VNF are not well understood due to a dearth of analytical and numerical modeling in this region of the plume. Most numerical modeling currently does not include the effects of the magnetic field[∀] and assumes the electrons are isothermal.[27] While these assumptions are sufficient to obtain excellent agreement far from the thruster, they do not adequately capture the plume evolution in the VNF. This was demonstrated by VanGilder, who compared results from an isothermal model to data that included a variable electron temperature that had been obtained by a fit to experimental data.[28] When the electron temperature was allowed to vary, the beam reached the thruster centerline in a shorter axial distance then the isothermal model. Keidar has considered the effects of the magnetic field beyond the VNF.[29] A strong magnetic field was shown to increase the plasma potential far from the thruster, which corresponded to experimental measurements. Neither of these studies offers a precise explanation of the trends observed in the 173Mv2 experiments. However, they do suggest that the influence of the electron dynamics and magnetic field on the focusing properties of Hall thruster plumes should be further investigated through experiment and simulation.

Figure 10 highlights regions near the discharge chamber walls where the collected current was negative. The data is the same as in Figure 9; only the scale has been changed. The current was negative here for the opposite reason the probe became saturated on the chamber centerline, (as discussed in the previous section). This can be understood by considering results from other HETs: First, measurements in Ref. 9 have shown that on either side of the chamber walls, the plasma potential falls rapidly by tens of volts. Second, measurements in Ref. 11-12 have shown that the electron temperature does not change substantially across the channel width and near the walls. Thus, outside the discharge chamber walls of the 173Mv2, the effective repelling potential of the probe was reduced by the decline in plasma potential. The repelling potential was then not large enough to repel most of the 5–10 eV electrons and a negative current was collected.

In these regions, a larger probe bias would be necessary to sufficiently repel all the electrons, but this would also result in the collection of more CEX ions in regions where the ion density was low. A variable probe bias is therefore needed to account for the different regions of the plume. No opportunities to correct for the negative current

[∀] The magnetic field leaking from the inner coil is on the order of the magnetic field in the discharge chamber.

were available because this behavior was not observed until after the test was completed. To correct for the negative current when later integrating the current density profiles, it was decided to set these regions to a value of zero. This was justified by reasoning that in these regions, which did not amount to a large area of the entire domain, the high-energy ion beam was absent. Thus, even if the probe bias had been much larger, the collected current would not contribute substantially to the total ion current calculation, which is discussed in the next section.

3. Calculating the total ion current

The integral of the ion current density from the thruster centerline as a function of radial position (at several different axial planes) is plotted in Figure 11. To compute the integral at each axial plane as a function of radius, the product of the ion current density at each radial position was multiplied by the differential area surrounding the point and then successively summed. The differential area of the nth measurement was defined by:[11]

$$A_n = \pi\left[\left(\frac{R_{n+1}+R_n}{2}\right)^2 - \left(\frac{R_n+R_{n-1}}{2}\right)^2\right] \quad \textbf{(3)}$$

The contribution of the CEX current to the integral can be a source of error. The contribution was evident because without some correction for CEX the integrated profiles continually increase with the radius (not shown). To correct for CEX, it was assumed that the ion current density collected at r = 300 mm (and a given axial coordinate) was due to CEX. This value was then subtracted from every point along the radial extent of integration. Measurements in Ref. 30 of CEX ions (using a backward facing Faraday probe) show an angular dependence of the CEX current density far from the SPT-100 exit plane that peaked on the thruster centerline. Thus, the approach adopted here should under-predict the CEX current density at most points in the plume.

The CEX population was apparently much higher than might be expected in regions before the energetic ion beam reached the thruster centerline (z = 0–75 mm, see Figure 10). Between z = 0–75 mm, it was highly unlikely that high-energy beam ions from the discharge chamber could reach the centerline in significant numbers. However, low-energy CEX ions could be trapped in the relatively high magnetic fields emanating from the inner coil, which would account for the elevated current density between z = 0–75 mm. If this was the case, the centerline CEX population was large enough that the z = 50 mm integral exceeded the discharge current before reaching the outer wall of the discharge chamber. The total integrated current began to drop after z = 75 mm, which was the likely result of beam expansion and cosine losses.

The purpose of Figure 11 was to determine an axial plane at which to compute the total ion current. For reasons discussed below, the Figure 11 data suggest that an estimate of the total ion current is possible by performing the integration at or near the cathode plane. At the cathode plane (z = +30 mm), the total ion current (I_i) integrated to 3.41 A. Since the discharge current (I_d) was 4.44 A, the ion current fraction was $I_i/I_d = 0.77$. The ion current fraction usually falls in the range of 0.7–0.8 in HETs.[18,31]

The choice of the cathode plane seemed appropriate for three reasons: First, at this axial location the beam divergence was very small, so the contribution to the total ion current past the outer wall should be negligible (shown in Figure 11). Second, an integration plane near the thruster exit reduced the effects of CEX and elastic scattering collisions in the plume. Third, at z = +30 mm, the area over which negative current was collected in Figure 10 was smaller than at axial locations less than z = +30 mm. Presumably, this was because the electron temperature decreased enough with axial distance so that the repelling potential of the probe was sufficient to reject most electrons.[11-12] Because of the larger negative regions at z = +20 and +25 mm, these planes integrate to only 3.11 A (70% of the discharge current). Estimates of the size of the negative region and an expected ion current density of ~1 mA/cm^2 showed that the 0.3 A difference between z = +20–25 and z = +30 mm can be accounted for. Therefore, if a suitable probe bias can be determined, it should be possible to integrate to the same ion current over the range of z = 10–30 mm. Additional data at multiple thruster conditions and variable probe biases are required to more accurately assess the utility of this diagnostic.

IV. CONCLUSIONS

The floating potential measurements have proven to be useful in understanding relative trends in the acceleration process. The most important result was the acceleration layer shifting 3±1 mm towards the anode as the voltage changed from 300 V to 600 V. Additionally, the acceleration layer was found to be 14±2 mm long and approximately constant with voltage and magnetic field. An external trim coil has also been shown to affect the

very-near-field structure of the potential distribution, which likely improved the coupling of the electrons with the discharge.

The ion current density measurements yielded insight on the evolution of the very-near-field plume. The annular ion beam was found to cross the thruster centerline 163 mm downstream of the exit plane. Comparison with data from other thrusters showed good agreement with the radial ion velocity required for convergence at this location. Analysis of the ion current density far from the thruster also showed that the radial velocity decreased substantially after the centerline crossing. The cathode plane has been identified as a suitable location for integrating ion current density profiles to yield the total ion current. At 500 V, 5 mg/s, the ion current fraction was calculated as 0.77, which was in the expected range of 0.7–0.8. The accuracy of this diagnostic can be improved by considering variable probe bias and methods to more accurately account for charge-exchange ions.

ACKNOWLEDGEMENTS

Support of this research by the NASA Glenn Research Center through grant NAG3-2307 (David Jacobson, technical monitor) is greatly appreciated.

Additionally, a debt of gratitude is owed to Dan Herman and Peter Peterson for sharing their experience and knowledge in the use of the HARP. The work Mr. Herman has done at PEPL (establishing automated DAQ with the HARP) is also greatly appreciated.

REFERENCES

1. Jankovsky, R. S, Jacobson, D. T., Sarmiento, C. J., Pinero, L. R., Manzella, D. H., Hofer, R. R., Peterson, P. Y., "NASA's Hall Thruster Program 2002," AIAA-2002-3675, 38th Joint Propulsion Conference, Indianapolis, IN, July 7-10, 2002.
2. Manzella, D. H., Jankovsky, R. S., Hofer, R. R., "Laboratory Model 50 kW Hall Thruster," AIAA-2002-3676, 38th Joint Propulsion Conference, Indianapolis, IN, July 7-10, 2002
3. Jacobson, D. T., Jankovsky, R. S., Rawlin, V. K., Manzella, D. H., "High Voltage TAL Performance," AIAA-2001-3777, 37th Joint Propulsion Conference, Salt Lake City, UT, July 8-11, 2001.
4. Hofer, R. R., Gallimore, A. D., "The Role of Magnetic Field Topography in Improving the Performance of High-Voltage Hall Thrusters," AIAA-2002-4111, 38th Joint Propulsion Conference, Indianapolis, IN, July 7-10, 2002.
5. Hofer, R. R., Jankovsky, R. S., "The Influence of Current Density and Magnetic Field Topography in Optimizing the Performance, Divergence, and Plasma Oscillations of High Specific Impulse Hall Thrusters," IEPC-03-142, 28th International Electric Propulsion Conference, Toulouse, France, March 17-21, 2003.
6. Manzella, D. H., Jacobson, D. T., Jankovsky, R. S., "High Voltage SPT Performance," AIAA-2001-3774, 37th Joint Propulsion Conference, Salt Lake City, UT, July 8-11, 2001.
7. Pote, B., Tedrake, R., "Performance of a High Specific Impulse Hall Thruster," IEPC-01-035, 27th International Electric Propulsion Conference, Pasadena, CA, Oct 14-19, 2001.
8. Haas, J. M., Gallimore, A. D., McFall, K., Spanjers, G., "Development of a High-speed, Reciprocating Electrostatic Probe System for Hall Thruster Interrogation," Review of Scientific Instruments, Vol. 71, No. 11, Nov. 2000.
9. Haas, J. M., Gallimore, A. D., "Internal Plasma Potential Profiles in a Laboratory-Model Hall Thruster," Physics of Plasmas, Vol. 8, No. 2, Feb 2001.
10. Haas, J. M., Gallimore, A. D., "Considerations on the Role of the Hall Current in a Laboratory-Model Thruster," IEEE Transactions on Plasma Science, Vol. 30, No. 2, April 2002.
11. Domonkos, M. T., Gallimore, A.D., Marrese, C. M., Haas, J. M., "Very-Near-Field Plume Investigation of the Anode Layer Thruster," Journal of Propulsion and Power, Vol. 16, No. 1, Jan-Feb 2000.
12. Kim, S. W., "Experimental Investigations of Plasma Parameters and Species-Dependent Ion Energy Distribution in the Plasma Exhaust Plume of a Hall Thruster," Ph.D. Dissertation, University of Michigan, 1999.
13. Esipchuk, Y. B, Morozov, A. I., Tilinin, G. N., Trofimov, A. V., "Plasma Oscillations in Closed-Drift Accelerators with an Extended Acceleration Zone," Soviet Physics – Technical Physics, Vol. 18, No. 7, January 1974.
14. Bishaev, A. M., Kim, V., "Local Plasma Properties in a Hall-Current Accelerator with an Extended Acceleration Zone," Soviet Physics – Technical Physics, Vol. 23, No. 9, September 1978.
15. Raitses, Y., Ashkenazy, J., Appelbaum, G., "Probe Measurements of Plasma Properties Inside an Experimental Hall Thruster," AIAA-

98-3640, 34th Joint Propulsion Conference, Cleveland, OH, July 13-15, 1998.
16. Kim, V., et al., "Local Plasma Parameter Measurements by Nearwall Probes Inside the SPT Accelerating Channel Under Thruster Operation with Kr," AIAA-2002-4108, 38th Joint Propulsion Conference, Indianapolis, IN, July 7-10, 2002.
17. Hutchinson, I. H., Principles of Plasma Diagnostics, Cambridge University Press, New York, 1987.
18. Kim, V., "Main Physical Features and Processes Determining the Performance of Stationary Plasma Thrusters," Journal of Propulsion and Power, Vol. 14, No. 5, Sept-Oct, 1998, pp. 736-743.
19. Hagstrum, H. D., "Auger Ejection of Electrons from Tungsten by Noble Gas Ion," Physical Review, Vol. 96, No. 2., pp. 325-335, 1954.
20. Hofer, R. R., Peterson, P. Y., Gallimore, A. D., "Characterizing Vacuum Facility Backpressure Effects on the Performance of a Hall Thruster," IEPC-01-045, 27th International Electric Propulsion Conference, Pasadena, CA, Oct 14-19, 2001.
21. Hofer, R. R., Peterson, P. Y., Gallimore, A. D., "A High Specific Impulse Two-Stage Hall Thruster with Plasma Lens Focusing," IEPC-01-036, 27th International Electric Propulsion Conference, Pasadena, CA, Oct 14-19, 2001.
22. Belan, N. V., Kim, V. P., Oranskiy, A. I., Tikhonov, V.B., "Statsionarnyye Plasmennyye Dvigateli," Khar'kov Khar'kovskiy Aviatsionnyy Institut, 1989. (In Russian)
23. Mason, L. S., Jankovsky, R. S., Manzella, D. H., "1000 Hours of Testing on a 10 Kilowatt Hall Effect Thruster," AIAA-2001-3773, 37th Joint Propulsion Conference, Salt Lake City, UT, July 8-11, 2001.
24. Walker, M. L., Hofer, R. R., Gallimore, A. D., "The Effects of Nude Faraday Probe Design and Vacuum Facility Backpressure on the Measured Ion Current Density Profile of Hall Thruster Plumes," AIAA-2002-4253, 38th Joint Propulsion Conference, Indianapolis, IN, July 7-10, 2002.
25. Prioul, M., et al., "Insights on Physics of Hall Thrusters through Fast Current Interruptions and Discharge Transients," IEPC-01-059, 27th International Electric Propulsion Conference, Pasadena, CA, Oct 14-19, 2001.
26. Smith, T. B., Herman, D. A., Gallimore, A. D., Drake, R. P., "Deconvolution of Axial Velocity Distributions from Hall Thruster LIF Spectra," IEPC-01-019, 27th International Electric Propulsion Conference, Pasadena, CA, Oct 14-19, 2001.
27. Boyd, I. D., "A Review of Hall Thruster Plume Modeling," AIAA-2000-0466, 38th Aerospace Sciences Meeting and Exhibit, Reno, NV, Jan 10-13, 2000.
28. VanGilder, D. B., Boyd, I. D., Keidar, M., "Particle Simulations of a Hall Thruster Plume," Journal of Spacecraft and Rockets, Vol. 37, No. 1, Jan-Feb 2000.
29. Keidar, M., Boyd, I. D., "Effect of a Magnetic Field on the Plasma Plume from Hall Thrusters," Journal of Applied Physics, Vol. 86, No. 9, November 1, 1999.
30. King, L. B., Gallimore, A. D., Marrese, C. M., "Transport-Property Measurements in the Plume of an SPT-100 Hall Thruster," Journal of Propulsion and Power, Vol. 14, No. 3, May-June 1998.
31. Hofer, R. R., and Jankovsky, R. S., "A Hall Thruster Performance Model Incorporating the Effects of a Multiply-Charged Plasma," AIAA-2001-3322, 37th Joint Propulsion Conference, Salt Lake City, UT, July 9-11, 2001.

Figure 1 – Photograph of the NASA-173Mv2 Hall effect thruster.

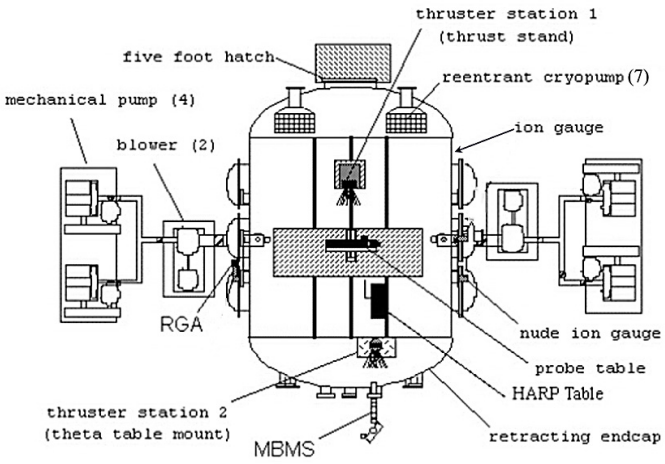

Figure 2 – Schematic of the Large Vacuum Test Facility (LVTF) at the University of Michigan.

Table 1 – Thruster telemetry from floating potential and ion current density measurements. Thrust, specific impulse, and efficiency from Ref. 5 are for reference only.

Label	Vd (V)	Id (A)	Anode (mg/s)	Cathode (mg/s)	IC (A)	OC (A)	ITC (A)	ETC (A)	Vcg (V)	Thrust (mN)	Total Specific Impulse (s)	Total Efficiency
Thruster Telemetry for Floating Potential Measurements (Four Cryopumps)												
300 V, No TC	300	9.20	10.00	1.00	1.75	1.50	0.00	0.00	-12.5	174.6	1620	0.511
300 V, ITC	300	9.00	10.00	1.00	1.75	1.50	-0.54	0.00	-12.6	174.9	1620	0.520
300 V, ITC, ETC	300	9.10	10.00	1.00	1.75	1.50	-0.54	-4.00	-14.4	176.3	1630	0.527
600 V, No TC	600	9.80	10.00	1.00	3.26	2.51	0.00	0.00	-15.0	269.9	2500	0.574
600 V, ITC	600	9.80	10.00	1.00	3.26	2.51	-0.26	0.00	-14.2	271.0	2510	0.580
600 V, ITC, ETC	600	9.90	10.00	1.00	3.26	2.51	-0.26	-5.00	-15.5	270.8	2510	0.580
Thruster Telemetry for Ion Current Density Measurements (Seven Cryopumps)												
300 V, No TC	300	4.18	5.00	1.00	1.50	1.20	0.00	0.00	-14.5	81.2	1510	0.471
500 V, No TC	500	4.44	5.00	0.50	1.56	1.46	0.00	0.00	-14.4	115.1	2140	0.543

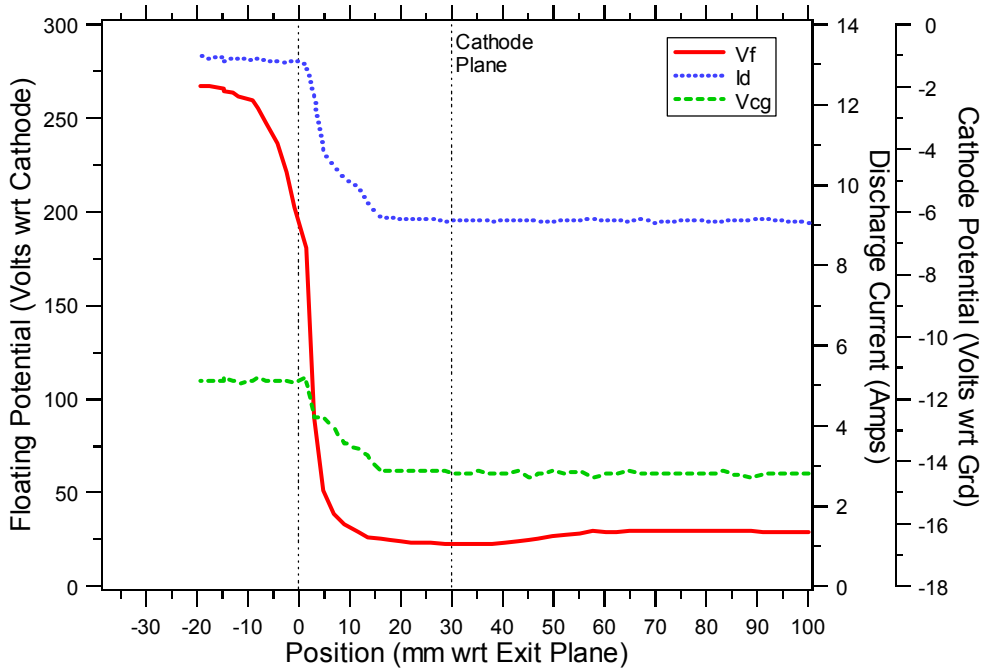

Figure 3 – Floating potential, discharge current, and cathode potential versus axial position at 300 V, 10 mg/s with both trim coils energized. Position was referenced from the exit plane, with the anode at z = –38 mm (the left vertical axis) and the cathode plane at z = +30 mm. The axial sweeps were taken on discharge chamber centerline (r = 73.7 mm).

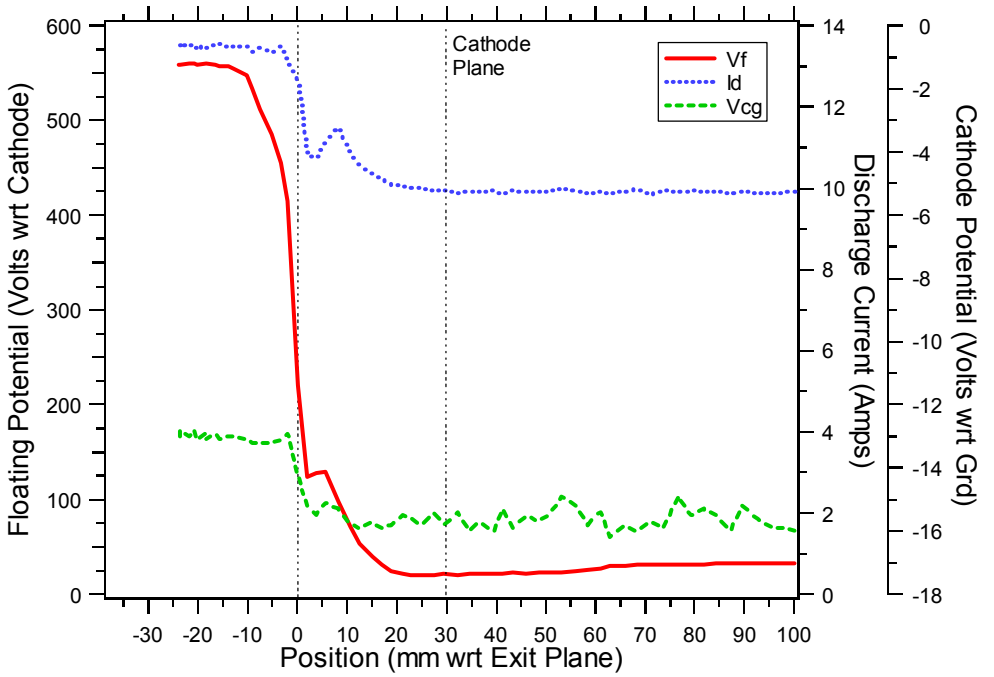

Figure 4 – Floating potential, discharge current, and cathode potential versus axial position at 600 V, 10 mg/s with both trim coils energized. Position was referenced from the exit plane, with the anode at z = –38 mm (the left vertical axis) and the cathode plane at z = +30 mm. The axial sweeps were taken on discharge chamber centerline (r = 73.7 mm).

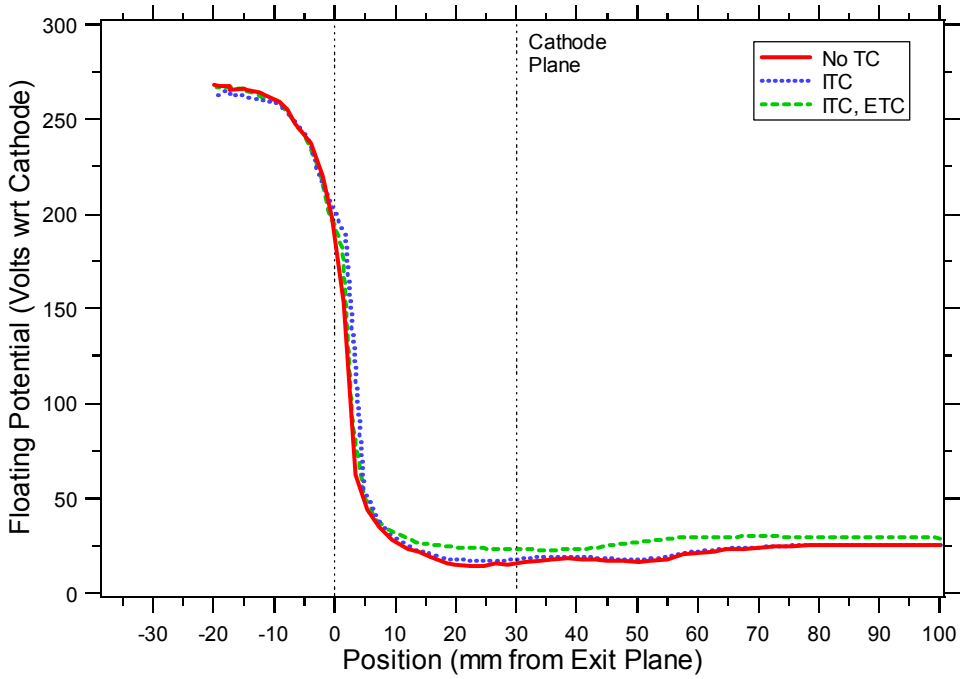

Figure 5 – Floating potential versus axial position at 300 V, 10 mg/s and different coil combinations. Position was referenced from the exit plane, with the anode at z = –38 mm (the left vertical axis) and the cathode plane at z = +30 mm. The axial sweeps were taken on discharge chamber centerline (r = 73.7 mm).

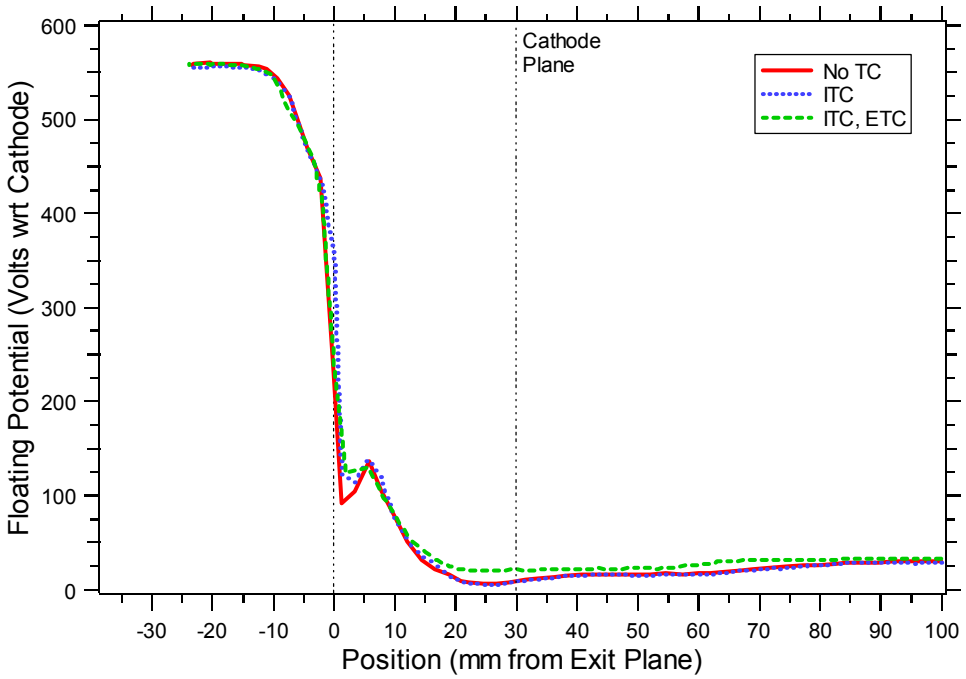

Figure 6 – Floating potential versus axial position at 600 V, 10 mg/s and different coil combinations. Position was referenced from the exit plane, with the anode at z = –38 mm (the left vertical axis) and the cathode plane at z = +30 mm. The axial sweeps were taken on discharge chamber centerline (r = 73.7 mm).

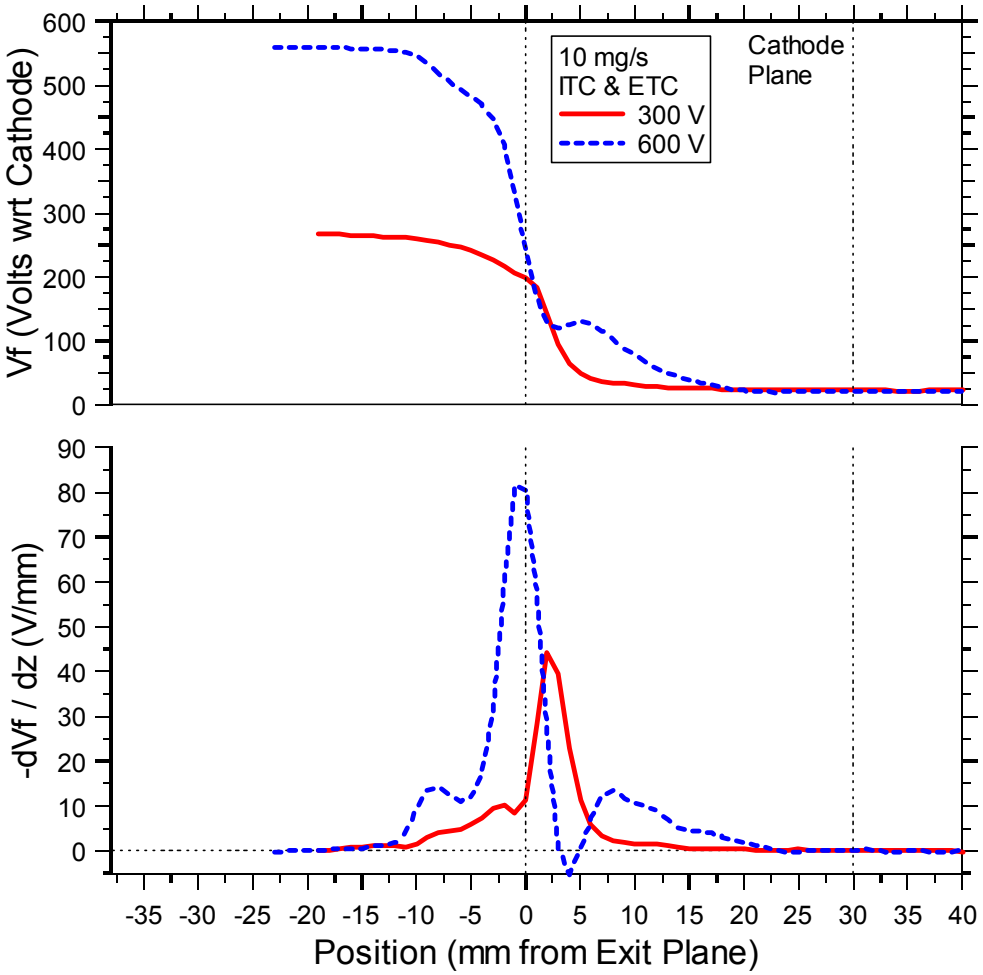

Figure 7 – Floating potential and its' negative first derivative ($-dV_f/dz$) versus axial position at 300 and 600 V with both trim coils (ITC, ETC). Position was referenced from the exit plane, with the anode at z = –38 mm (the left vertical axis) and the cathode plane at z = +30 mm. The axial sweeps were taken on discharge chamber centerline (r = 73.7 mm).

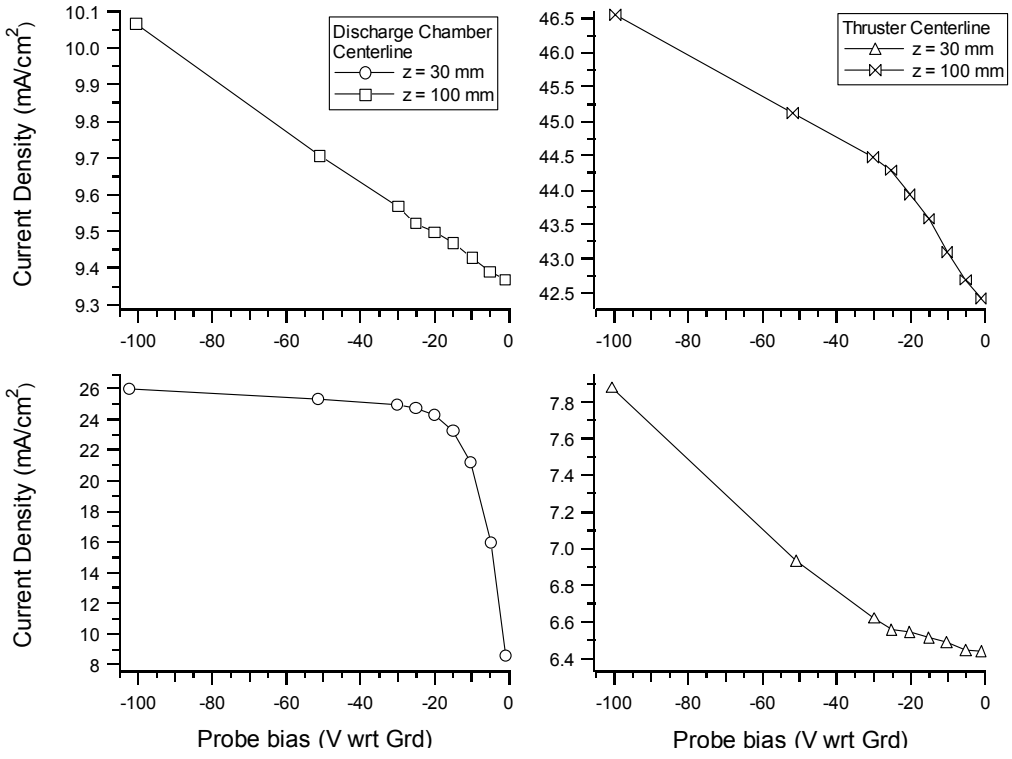

Figure 8 – Partial results from the probe saturation study at 300 V, 5 mg/s, without trim coils.

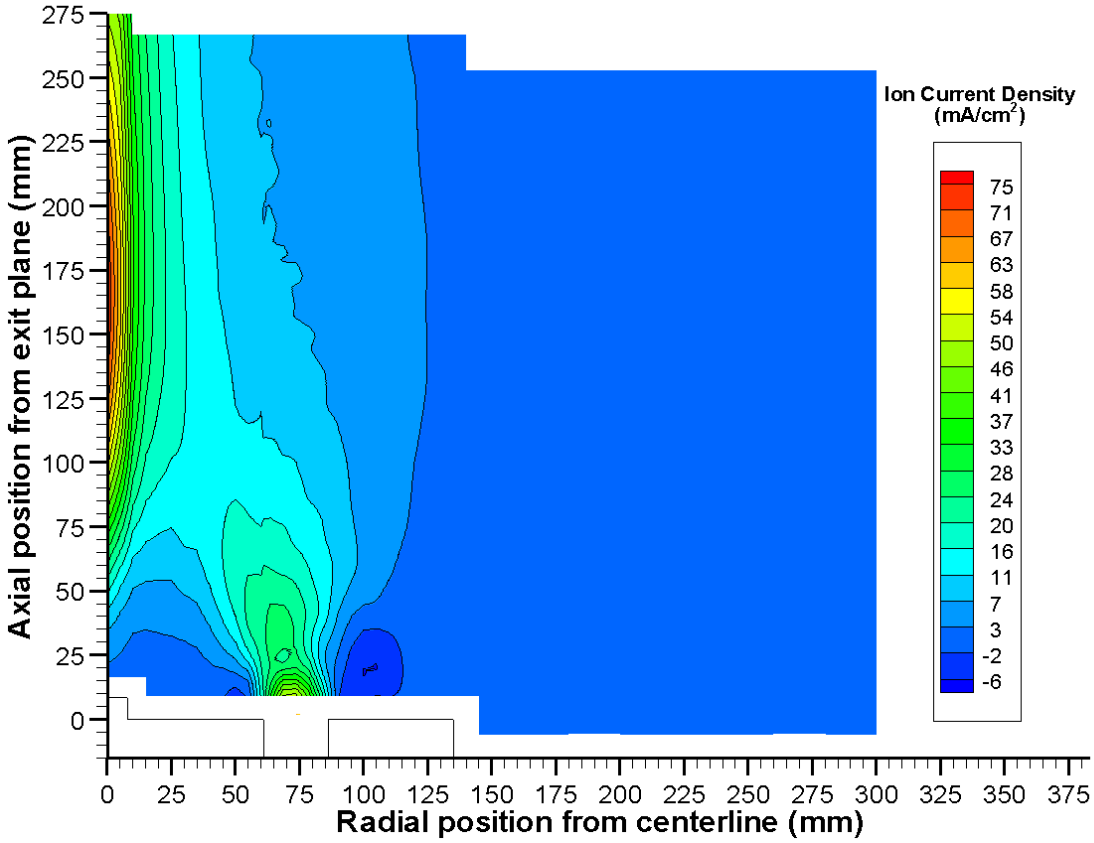

Figure 9 – Contours of ion current density at 500 V, 5 mg/s, without trim coils. An explanation for negative current collection is given at the end of section III.B.2.

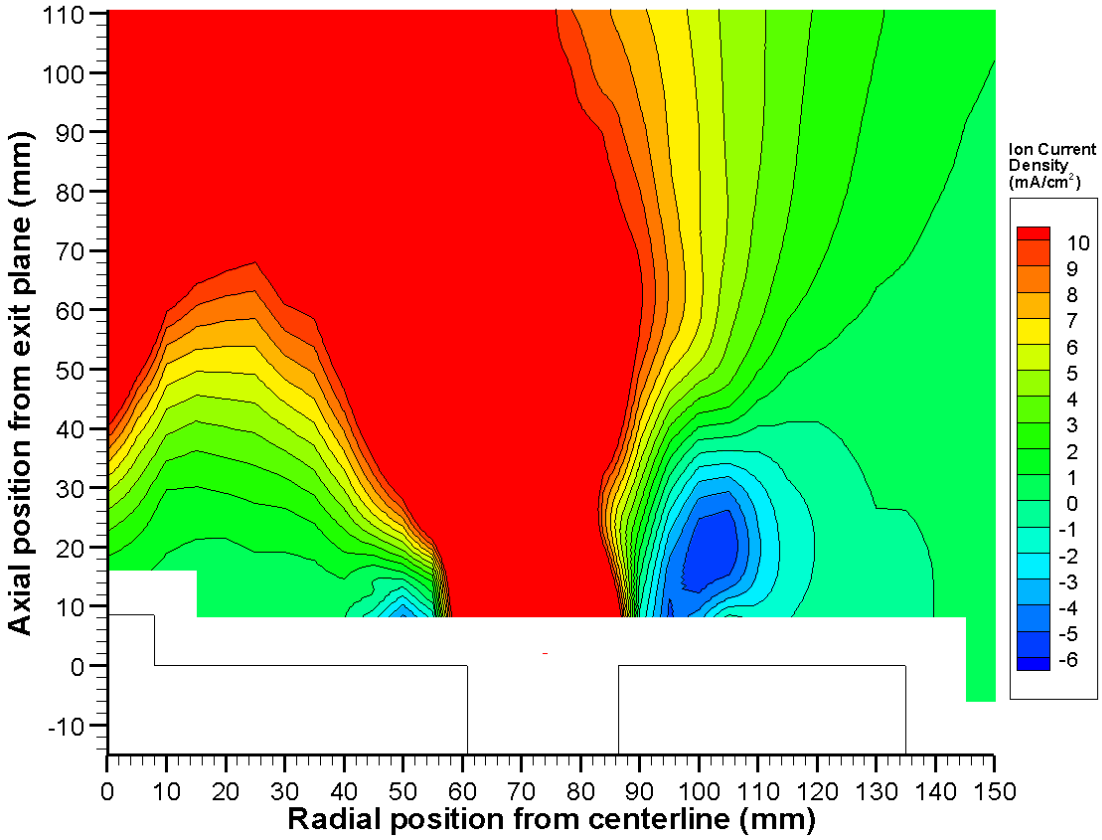

Figure 10 – Close-up of ion current density contours from Figure 9 at 500 V, 5 mg/s, without trim coils, flooded so that the regions where the current was negative are highlighted. An explanation for negative current collection is given at the end of section III.B.2.

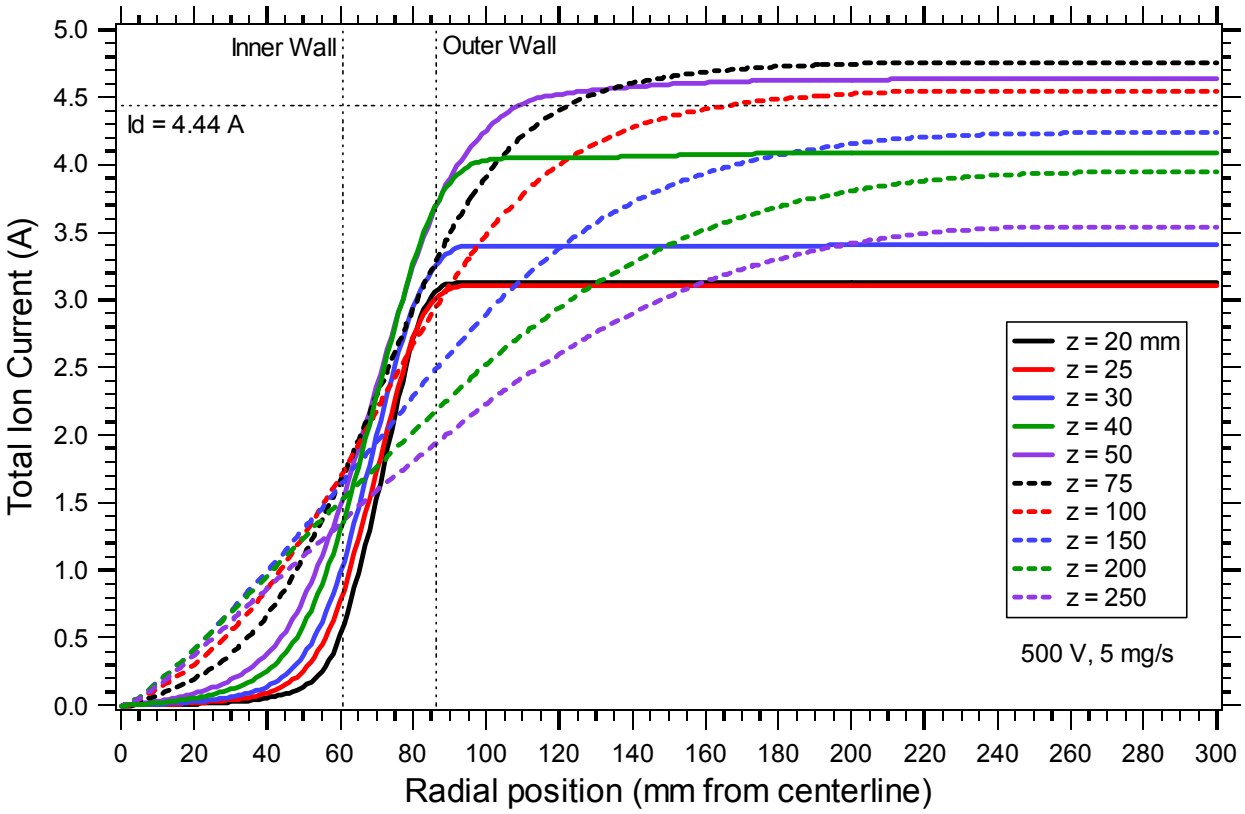

Figure 11 – Integral of the ion current density versus radial position at 500 V, 5 mg/s, without trim coils. Results from several axial positions from the thruster exit plane are shown. Vertical lines indicate the location of the discharge chamber walls and the discharge current is indicated with a horizontal line.